

Low Fidelity Visuo-Tactile Pretraining Improves Vision-Only Manipulation Performance

Selam Gano

Department of Mechanical Engineering
Carnegie Mellon University United States
selamg@andrew.cmu.edu

Abraham George

Department of Mechanical Engineering
Carnegie Mellon University United States
aigeorge@andrew.cmu.edu

Amir Barati Farimani

Department of Mechanical Engineering
Carnegie Mellon University United States
barati@andrew.cmu.edu

Abstract: Tactile perception is a critical component of solving real-world manipulation tasks, but tactile sensors for manipulation have barriers to use such as fragility and cost. In this work, we engage a robust, low-cost tactile sensor, BeadSight, as an alternative to precise pre-calibrated sensors for a pretraining approach to manipulation. We show that tactile pretraining, even with a low-fidelity sensor as BeadSight, can improve an imitation learning agent’s performance on complex manipulation tasks. We demonstrate this method against a baseline USB cable plugging task, previously achieved with a much higher precision GelSight sensor as the tactile input to pretraining. Our best BeadSight pretrained visuo-tactile agent completed the task with 70% accuracy compared to 85% for the best GelSight pretrained visuo-tactile agent, with vision-only inference for both. Code for this project is available at: <https://github.com/selamie/beadsight>

Keywords: Tactile sensing, robotic manipulation, contrastive pretraining, imitation learning

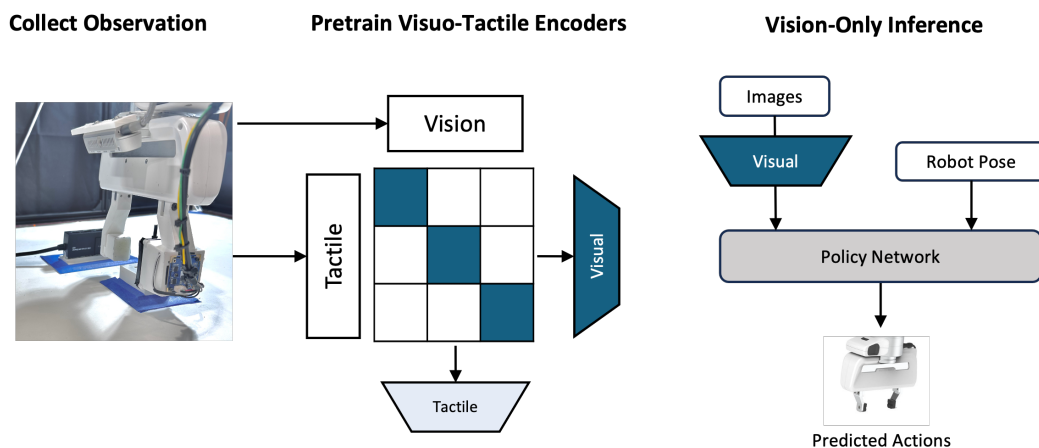


Figure 1: Our method uses a low-fidelity tactile sensor for pretraining. Contrastive tactile-vision observation pretraining produces a visual encoder well-aligned to tactile observations that is then fine-tuned on the actual action sequence prediction task. Finally, vision-only performance at inference is improved using the residual tactile influence of the pretrained encoder.

1 Introduction

Translating advances in visual perception to robotic grasping and manipulation of objects remains challenging. For complex manipulation tasks such as peg insertion, pulling or twisting with resistance, and dynamic motions such as throwing and catching, fine-grained manipulation requires tactile perception. Tactile sensors have been paired with visual sensors for both classical control and machine learning approaches to these tasks [1], but issues of fragility and cost present barriers to heavy use or industrial integration, particularly for manipulation tasks that would place higher forces on sensors at the tactile edge.

Previously, a GelSight [2] tactile sensor was used to train an agent on a USB insertion task [3], the first time this was achieved with imitation learning. GelSight is not designed for robustness to higher shear forces and was noted to break irrecoverably during data collection and inference for that task, requiring repeated replacement. This work also demonstrated an approach using tactile information only during pretraining, then ablating the tactile sensor at inference, achieving a more robust vision-only manipulation system.

BeadSight [4] aimed to make a simpler, low cost calibration-free sensor that, like GelSight, still operated at an end effector’s point of contact with objects. We constructed the BeadSight sensor, which does not rely on any calibration and instead relies entirely on neural networks to distill information about contacts and movements at the tactile edge.

In this work, we repeated the visuo-tactile pretraining USB plugging experiment using the much lower fidelity BeadSight to produce a direct comparison with the GelSight sensor in the task of plugging in a USB cable. Our contributions are:

1. We demonstrate the effectiveness of visuo-tactile pretraining even with a lower fidelity, imprecise sensor on two different state-of-the-art imitation learning methods.
2. We demonstrate an affordable durable approach to visuo-tactile pretraining, which is especially cost-effective for improving the performance of vision-only agents.
3. We show that by freezing a pretrained tactile encoder, we can mitigate the overfitting of low-fidelity tactile sensors.

2 Background and Related Work

2.1 Tactile Sensing

In robotic manipulation, there are a wide variety of tactile sensors and sensing approaches [1]. These sensors use different modalities to collect tactile information, including forces and torques applied normally or tangentially [5] [6], mechanical vibrations [7] [8], thermal measurement and conductivity [9] [10], and pre-touch proximity [11].

Tactile image processing with machine learning and traditional image-based approaches have been used successfully with visuo-tactile sensors that use a camera near the point of contact, with most tracking the deformation of some surface [1]. This paper will focus on the visuo-tactile category of sensors and approaches, which include cameras placed directly on robot fingertips [2], and sensors like DenseTact [12] [13], See-Through-Your-Skin [14], and GelSight [15].

The GelSight sensor is designed to measure geometry with a very high spatial resolution, such that the deformation of its gel-elastomer surface corresponds directly to the exact object shape and tension on the contact surface [15]. Markers printed on the gel surface are tracked by an embedded camera, which can estimate shear force and slip state. Deriving exact measurements from GelSight requires an initial calibration step. Previous work using a GelSight Mini for the same task of plugging in a USB cable noted the fragility of the elastomer gel and the sensor itself for tasks that apply higher forces to the contact surface [3].

BeadSight is a low-cost visuo-tactile sensor that uses hydrogel beads as an inexpensive, durable sensing medium [3]. This deformable surface is inexpensive and durable, with an embedded camera observing the beads’ motion and deformation. However, the beads’ movements are stochastic and, unlike GelSight, the relationship between the beads and shear forces cannot be directly resolved with analytical methods. Previously, a deep neural network was used to reconstruct contact pressure maps with BeadSight as an example tactile learning approach.

2.2 Tactile Sensing and Manipulation Control Policies

Prior work integrating tactile sensors in control policies range from classical control approaches to reinforcement and imitation learning. [16] used classical state estimation and a heuristic method to follow cables and insert wires. [17] combined a linear-quadratic regulator (LQR) controller and linear dynamics model to follow an audio cable and successfully plug in a headphone jack. Reinforcement Learning (RL) agents have been trained to perform peg insertion, door opening, and in-hand rotation tasks [18, 19]. These approaches require simulation for the sheer amount of training required (~ 1 million steps). Nearest Neighbors Imitation Learning [20] is a method that encodes observations and demonstrations into a latent space and compares the distance between them; [21] used this method with online residual reinforcement learning to reduce computation intensity and learn visuo-tactile peg insertion. [22] used a similar approach to learn a variety of tasks including bowl and cup unstacking, bottle opening, and joystick movement.

2.3 Imitation Learning Methods

Imitation Learning (IL) methods aim to mimic human behavior by learning from human demonstrations, which can be easier than designing optimal reward functions as in reinforcement learning [23]. Variations of this method have trained manipulation agents to perform kitchen tasks and stack blocks [24, 25] and even sculpt clay [26]. IL tends to perform more poorly for more complex action sequences, particularly with non-deterministic goal policies and significant shifts between training and deployment domains. We focus on state of the art methods that aim to address these drawbacks, Action Chunking Transformers (ACT) [27] and Diffusion Policy [28]. ACT uses a temporal ensembling approach to maintain a consistent action trajectory in spite of out-of-distribution observations, and Diffusion Policy uses diffusion to better model multi-modal action pathways.

2.3.1 Diffusion Policy

Prior work in [28] constructs a diffusion framework that generates observation-conditioned action sequences, $p(\mathbf{O}_t|\mathbf{A}_t)$, where action sequence \mathbf{A}_t is conditioned on \mathbf{O}_t , an observation at timestep t . A sample of examples \mathbf{A}_t^0 is drawn from the dataset during training, and a random noise ϵ^k is sampled for denoising step k . The noise prediction network ϵ_θ predicts noise from the noised example data using the loss function:

$$Loss = MSE(\epsilon^k, \epsilon_\theta(\mathbf{O}_t, \mathbf{A}_t^0 + \epsilon^k, k))$$

The denoising diffusion model [29] iteratively denoises a Gaussian sample representing the action sequence:

$$\mathbf{A}_t^{k-1} = \alpha(\mathbf{A}_t^k - \gamma\epsilon_\theta(\mathbf{O}_t, \mathbf{A}_t^k, k) + \mathcal{N}(0, \sigma^2 I))$$

Feature-Wise Linear Modulation (FiLM) layers in the noise prediction network enable a conditioning encoder to influence the network [30]; observation \mathbf{O}_t is used to condition the denoising process this way.

2.3.2 Action Chunking Transformers (ACT)

ACT trains a Conditional Variational Autoencoder (CVAE) combined with a transformer backbone to predict action sequences conditioned on state and vision observations [27]. During training, the latent variable of the CVAE helps the model capture multi-modal policies, while a large KL divergence loss keeps the network from becoming too reliant on the latent information. During inference, the latent variable is set to zero. The autoencoder uses a latent variable to reduce the impact of multi-modal training data, and temporal ensembling at inference reduces the effect of a single bad prediction. Specifically, ACT predicts the goal states A_t to A_{t+h} at each timestep. During inference, the previous predictions A_{t-h} to A_{t-1} are combined with current predictions using a weighted average of exponentially decaying weights, $w_i = e^{-ki}$. These “ensembled” actions are then executed.

2.4 Contrastive Pretraining

Contrastive pretraining methods train models to distinguish between similar and dissimilar data, coding them as positive (similar) or negative (dissimilar) pairs [31]. Those modeled after the structure of Contrastive Language Image Pretraining (CLIP) [32] do this by maximizing the cosine similarity of the paired data in some multimodal embedding space, while minimizing the similarity of dissimilar pairs. For visuo-tactile robotic manipulation, tactile and visual observations can be compared in that latent space. [33] used this approach to better identify flaws in fabric, and [34, 35] both improved visuo-tactile object identification this way.

3 Methods

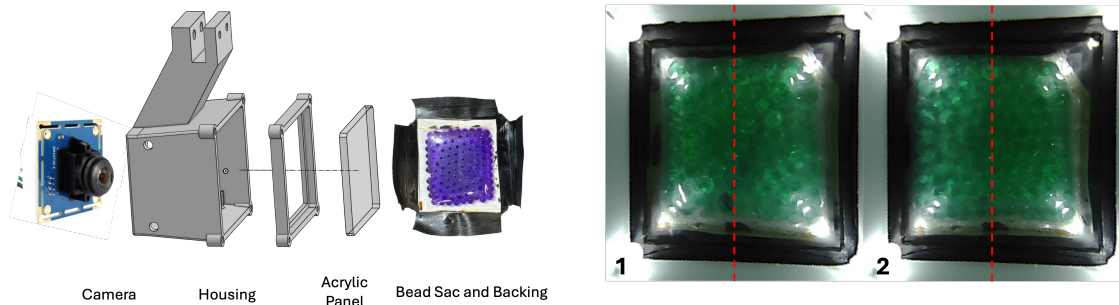


Figure 2: Left, BeadSight components and construction. Slight modifications were made to the original enclosure to better manipulate objects, including the robot gripper mount and a separate housing lid to create a secure, interchangeable deformable surface. Right, the embedded camera’s view of the BeadSight hydro-gel bead sac, relaxed (1) and being pressed (2), after down-scaling and correcting fish eye distortion.

3.1 BeadSight Hardware

The version of BeadSight used for this work was constructed in a multi-part design that separated the deformed surface, camera, and contact surface. The BeadSight enclosure is a 3D printed body with threaded heat inserts on attachment points, and includes a mount that attaches the body to the Franka Emika Panda robot gripper. A “lid” allows easy separation of an interchangeable contact surface, making the system repairable for long-term wear and tear. The lid consists of a 3D printed frame, press-fit acrylic insert, and a hydro-gel bead sac. The hydro-gel bead sac is backed with white adhesive tape to reflect light back to the camera and improve visibility of the deformation. Black Polyvinyl Chloride (PVC) adhesive tape is the final layer on the hydro-gel bead sac, sealing the sensor from external light sources.

The hydro-gel bead sacs themselves are of the same construction as [4], using Polyacrylamide (PAM) beads that are hydrated with water and sealed in clear PVC sheeting. For the data in this work, the bead sac used about 50 green PAM beads hydrated with 5ml of water. The embedded camera is also the same as in [4], a 1080×1920 USB camera with 180° fish eye lens. 4 LEDs illuminate the hydro-gel sac, with the camera capturing at 30Hz. The image frames from the camera are down-scaled to 480×480 resolution and the fish-eye is corrected before processing.

3.2 Data Collection

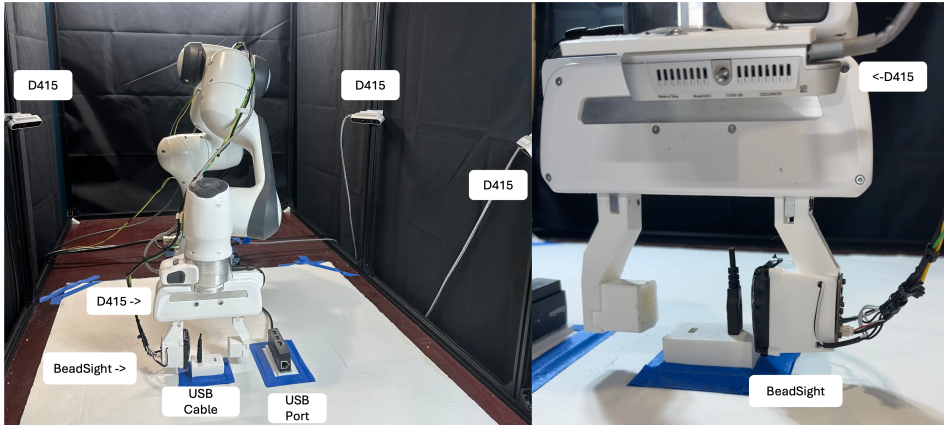


Figure 3: Experimental scene, with a D415 wrist camera (not visible) behind the robot gripper.

Our experimental setup recreated [3] in order to directly compare the performance of BeadSight and GelSight. To train ACT, Diffusion Policy, and the contrastive pretraining model, we used 105 expert demonstrations collected via teleoperation of a Franka Emika Panda robot. We used the Oculus Virtual Reality (VR) teleoperation method developed in [36] which uses handheld Oculus controllers to move the robot end-effector. Only motion control was done with the Oculus system; the human teleoperator looked directly at the workspace rather than through the VR headset.

Visual observations of the scene were collected by six Intel RealSense scene cameras. These consist of four D415 cameras mounted around the workspace, a D415 camera mounted at the robot’s wrist, and a D445 overview camera mounted on a top edge of the workspace frame. The BeadSight sensor mounted on the robot gripper fingers collected tactile observations. A parallel finger was 3D printed to match the BeadSight, with silicone gel on the surface to aid grip.

The experimental task consisted of a USB port hub, a holder for a USB plug, and the USB plug with friction tape applied to assist grip. The hub and holder were fixed for the duration of the experiments, as our goal was to evaluate the plug insertion itself rather than the ability to locate the plug or port. We collected 105 expert demonstrations of grasping the plug and inserting it into the USB port closest to the robot (a successful execution at inference must choose the same port).

3.3 Tactile Encoder

The hydro-gel beads are not fixed components, and therefore cannot record any exact tactile measurements. Instead, tactile events can be inferred from the beads’ relative motion and deformation over some period of time. To capture this relative motion, we introduce a “tactile horizon”, the total number of past tactile frames (including the current frame) combined to form the tactile observation. We use a tactile horizon of 5 frames (the current time step and four previous time steps). We collapse the 5 frames on the channel dimension, converting 5 individual $3 \times 480 \times 480$ images to a single $15 \times 480 \times 480$ tensor. For a different tactile horizon, the representative tensor would be of the shape $3h \times 480 \times 480$, where h is the horizon. This collapsed tensor allows us to add a single convolutional layer (converting 15 channels to 3 channels) to a pre-trained ResNet-18 [37] encoder as the encoder

for BeadSight. The classification layer is removed such that a given image is projected to a 512 embedding vector before being passed to the downstream model.

To provide a horizon for the first few time steps, the BeadSight tactile observation buffer is initialized with $h - 1$ duplicates of the initial tactile frame. For this task, the sensor is not in contact with any object or surface at the start of each task run, so we would expect the initial frames to be nearly identical.

3.3.1 Contrastive Pretraining

The vision and tactile encoders were pre-trained using the contrastive pretraining method described in [3]. This method leverages the relationships between the three different modalities of data our agent observes (visual, tactile, and positional) to train the encoders to extract task-relevant features. During pretraining, two projection networks are learned, one for visual observations, and one for tactile and positional observations. These projection networks consist of an encoder (ResNet-18 for the image encoder, and the BeadSight encoder described above for the tactile encoder), along with a projection head that casts the encoded observations to a shared latent embedding space. The positional information is also passed to the tactile projection head. By adding position information to the tactile projector, we ensure the resulting latent space has both global information (position observations) and local information (tactile observations).

To train the projection networks, a set of timesteps is sampled from a single trajectory, and the corresponding observations are projected to the shared latent space. Then, a CLIP loss is used to encourage the embeddings from the same timestep to be similar, while driving the projection of the observations from different timesteps. All of the camera views are encoded using a shared visual encoder. At each update, the contrastive loss is calculated separately for each camera and then summed, according to the equation:

$$loss = - \sum_c \sum_{i \in t} \frac{1}{2n} (\log(\frac{\exp(sim_{i,i,c}/\tau)}{\sum_{j \in t} \exp(sim_{i,j,c}/\tau)}) + \log(\frac{\exp(sim_{i,i,c}/\tau)}{\sum_{j \in t} \exp(sim_{j,i,c}/\tau)}))$$

Where $sim_{i,j,c}$ is the cosine similarity between the tactile embedding from timestep i and the visual embedding of camera c 's observation from timestep j .

3.3.2 Diffusion Policy

Our Diffusion Policy approach leveraged [28], and was modeled after [3], with similar baseline hyper-parameters. We used the 1-D temporal CNN implementation which was noted to be less sensitive to hyper-parameter tuning and train stably for most tasks. Diffusion Policy is most effective when each camera view uses a separate initial encoder, so 6 ResNet-18 encoders were constructed and fine-tuned during training, one for each scene camera. We remove the final ResNet-18 layer to project the image to a 512 embedding for the downstream model. For the pretrained model, six of the pretrained ResNet-18 vision encoders were constructed and separately fine-tuned during training.

After encoding, the vision and tactile observations were stacked to form a single observation vector, then passed to the network to condition its noise prediction. To compare directly to GelSight's performance in [3], we use the same settings of 1 observation horizon, an action prediction horizon of 20, and executed 8 timesteps out of the 20 available predictions at inference. We also took advantage of noise scheduler decoupling, using 100 denoising steps during training for better resolution but using only 10 inference steps for faster execution.

3.3.3 Action Chunking Transformers

We also used the same ACT architecture as [3], with the only change being the replacement of the GelSight encoder with the BeadSight encoder. ACT calculates a set of goal actions based on the robot's current position, the latent encoding of the goal action sequence (set to zero during inference), and the encoded visual and tactile observations. Unlike Diffusion Policy, ACT does not

	Pretrained, Tactile + Vision	Pretrained, Vision Only	Tactile + Vision	Vision Only	Pretrained, Tactile** + Vision	Tactile** + Vision
Diffusion (B)	0.05	0.7	0.1	0.05	0.8	0.2
ACT (B)	0.25	0.65	0.5	0.15	-	-
Diffusion (G)	0.75	0.75	0.7	0.45	-	-
ACT (G)	0.95	0.85	0.9	0.2	-	-

Table 1: Results of the USB cable plugging experiment, with (B) denoting the BeadSight and (G) showing the previous results with GelSight from [3]. ** Denotes that the tactile encoder is frozen.

apply an average adaptive pool to the output of the encoders, instead flattening the feature map to form an input sequence of shape ($len \times 512$). As with [3], we trained ACT on the relative position space, and at inference, implemented temporal ensembling in the global frame with temperature constant $k = 0.25$.

4 Experimental Results

To examine the effect of pretraining with a low-fidelity tactile sensor on imitation learning agents, we tested our trained ACT and diffusion agents on the cable plugging task described in Section 3.2, following the same evaluation criteria used in [3] so that we can directly compare our results. For each evaluation, the agent attempted the task 20 times, with success being recorded if the agent plugged in and then released the USB. To increase the difficulty of the task, random noise was applied to the goal action, sampled from a normal distribution with a standard deviation of 2.5 mm.

For both ACT and Diffusion Policy, we evaluated the effect of low fidelity visuo-tactile pretraining on both vision only agents and visuo-tactile agents. Our results, along with the evaluation using GelSight instead of BeadSight, can be seen in Table 1.

In the prior visuo-tactile pretraining experiments using GelSight, pretraining was found to increase the performance of both vision-only and visuo-tactile agents for both ACT and diffusion policy, although the improvement was more pronounced with the vision-only agents. However, replacing the GelSight with a low-cost, low-fidelity sensor reversed part of this trend. We found that pretraining significantly harmed the visuo-tactile agent’s performance, halving the success rate of both ACT and Diffusion Policy.

In contrast, visuo-tactile pretraining significantly improved the performance of the vision-only agent, allowing the vision-only policies to outpace the visuo-tactile policies for both ACT and Diffusion agents. We believe this counter-intuitive result, that less information led to an improvement in model performance, is likely due to the network overfitting to the BeadSight observations. Not only is the BeadSight stochastic, but the beads can undergo significant drift between experiments, leading to a train-test distribution mismatch. Also, overfitting would explain why Diffusion Policy is more negatively affected by BeadSight observation than ACT, as the temporal ensembling in ACT helps address out-of-distribution states. This resistance is especially important in tasks like cable plugging, where a single wrong action (such as opening the gripper at the wrong time) can lead to an irrevocable failure.

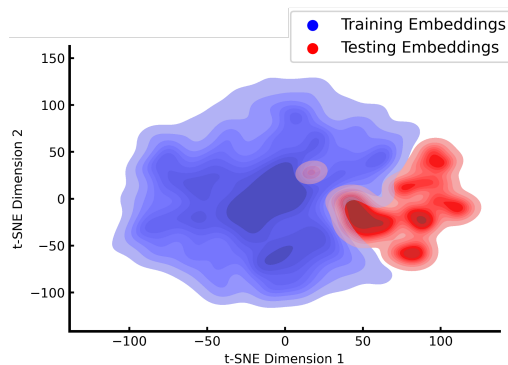


Figure 4: tSNE plot showing the distribution shift between training and deployment for the tactile observation.

To investigate BeadSight overfitting, we compared the BeadSight observations collected during training with those collected during model testing. We extracted the relevant tactile features using the tactile encoder from the pretraining step and graphed a tSNE plot [38] of the resulting BeadSight embeddings. This plot can be seen in Figure 4. The tSNE results show a clear divide between the training data set and the bead sight observations collected during testing, reflecting a significant train-test distribution shift, which can cause overfitting.

To address the agent’s overfitting to the BeadSight data, we froze the bead sight encoder weights before training the agents. For the pre-trained agent, these frozen weights were the result of the contrastive pretraining, while for the non-pretrained agent, the weights were frozen at initialization. Although this approach works for diffusion, where the encoder returns a single 512 vector, ACT removes the final pooling layer from the encoder passing the entire feature map (a 225x512 sequence) into the transformer, which we can’t freeze. To properly reduce overfitting via encoder freezing, we would need a narrower encoder bottleneck, which would require a significant alteration of the model. Therefore, to preserve consistency, we only evaluated this approach on the Diffusion model. The performance of these policies can be seen in Table 1. Our results show that freezing the weights reduced overfitting, causing a significant improvement in performance over the fine-tuned models and overtaking the performance of their respective vision-only and visuo-tactile counterparts.

Comparing these final results to those achieved in [3] using GelSight, we see that without pretraining, using a low-quality tactile sensor for imitation learning leads to a significant drop in performance. However, visuo-tactile pretraining, when combined with weight freezing, can help close this gap. When a vision-only policy is desired, then an inexpensive tactile sensor can be used.

5 Conclusion

In this work, we explored combining a low-fidelity tactile sensor (BeadSight) with pretraining for imitation learning. We found that using low-fidelity tactile sensors for imitation learning (without pretraining) results in a significant reduction in performance and is prone to overfitting. However, this performance deficit can be significantly reduced using contrastive pretraining. Also, by freezing the pre-trained weights, much of the overfitting issues can be resolved. Additionally, by using a low-fidelity tactile sensor and visuo-tactile pretraining, we were able to significantly improve the performance of a vision-only agent, replicating a prior finding that used a high-resolution GelSight tactile sensor.

These relative performance improvements used ~ 100 expert demonstrations and low computational intensity imitation learning methods. This suggests tactile pretraining can be another tool for improving manipulation performance on difficult tactile-rich tasks with efficient computational methods. Other work in IL has attempted to dramatically reduce the number of demonstrations necessary for an agent to imitate an action [39] and one can imagine tactile pretraining as a way to further improve IL’s efficiency on tactile-rich tasks.

Future work could explore adding on to the imitation learning pipeline proposed here. In addition to freezing the tactile encoder after pretraining, we may also explore encoding the tactile image in a latent space to improve tactile performance at inference. A latent vector produced by an autoencoder could be used as the tactile observation rather than the image of the bead sac directly. Tracking and masking out the image of the tactile sensor could allow any gripper finger used in deployment, improving utility of the vision-only agent. Finally, the benefit of freezing the encoder together with the pretraining approach implies a way to pretrain an encoder on a large, diverse dataset and use this to inform downstream tactile manipulation tasks, with only vision used at execution. This kind of pretrained model at an appropriate scale could broadly improve general robot manipulation.

Acknowledgments

References

- [1] Q. Li, O. Kroemer, Z. Su, F. F. Veiga, M. Kaboli, and H. J. Ritter. A review of tactile information: Perception and action through touch. *IEEE Transactions on Robotics*, 36(6):1619–1634, 2020.
- [2] A. Maldonado, H. Alvarez, and M. Beetz. Improving robot manipulation through fingertip perception. In *2012 IEEE/RSJ International Conference on Intelligent Robots and Systems*, pages 2947–2954. IEEE, 2012.
- [3] A. George, S. Gano, P. Katragadda, and A. B. Farimani. Visuo-tactile pretraining for cable plugging. *arXiv preprint arXiv:2403.11898*, 2024.
- [4] A. George, Y. Chen, A. Dikshit, P. Pak, and A. B. Farimani. Beadsight: An inexpensive tactile sensor using hydro-gel beads. *arXiv preprint arXiv:2405.13204*, 2024.
- [5] W.-C. Choi. Polymer micromachined flexible tactile sensor for three-axial loads detection. *Transactions on electrical and electronic materials*, 11(3):130–133, 2010.
- [6] C. Schurmann, R. Haschke, H. Ritter, et al. A modular high-speed tactile sensor for human manipulation research. In *2011 IEEE World Haptics Conference*, pages 339–344. IEEE, 2011.
- [7] M. Meier, G. Walck, R. Haschke, and H. J. Ritter. Distinguishing sliding from slipping during object pushing. In *2016 IEEE/RSJ International Conference on Intelligent Robots and Systems (IROS)*, pages 5579–5584. IEEE, 2016.
- [8] A. Molchanov, O. Kroemer, Z. Su, and G. S. Sukhatme. Contact localization on grasped objects using tactile sensing. In *2016 IEEE/RSJ International Conference on Intelligent Robots and Systems (IROS)*, pages 216–222. IEEE, 2016.
- [9] D. Siegel, I. Garabieta, and J. Hollerbach. An integrated tactile and thermal sensor. In *Proceedings. 1986 IEEE International Conference on Robotics and Automation*, volume 3, pages 1286–1291. IEEE, 1986.
- [10] J. Wade, T. Bhattacharjee, and C. C. Kemp. A handheld device for the in situ acquisition of multimodal tactile sensing data. *arXiv preprint arXiv:1511.03152*, 2015.
- [11] K. Koyama, M. Shimojo, T. Senoo, and M. Ishikawa. High-speed high-precision proximity sensor for detection of tilt, distance, and contact. *IEEE Robotics and Automation Letters*, 3(4): 3224–3231, 2018.
- [12] W. K. Do and M. Kennedy. Densetact: Optical tactile sensor for dense shape reconstruction. In *2022 International Conference on Robotics and Automation (ICRA)*, pages 6188–6194. IEEE, 2022.
- [13] W. K. Do, B. Jurewicz, and M. Kennedy. Densetact 2.0: Optical tactile sensor for shape and force reconstruction. In *2023 IEEE International Conference on Robotics and Automation (ICRA)*, pages 12549–12555. IEEE, 2023.
- [14] F. R. Hogan, M. Jenkin, S. Rezaei-Shoshtari, Y. Girdhar, D. Meger, and G. Dudek. Seeing through your skin: Recognizing objects with a novel visuotactile sensor. In *Proceedings of the IEEE/CVF Winter Conference on Applications of Computer Vision*, pages 1218–1227, 2021.
- [15] W. Yuan, S. Dong, and E. H. Adelson. Gelsight: High-resolution robot tactile sensors for estimating geometry and force. *Sensors*, 17(12):2762, 2017.
- [16] A. Wilson, H. Jiang, W. Lian, and W. Yuan. Cable routing and assembly using tactile-driven motion primitives. In *2023 IEEE International Conference on Robotics and Automation (ICRA)*, pages 10408–10414. IEEE, 2023.

- [17] Y. She, S. Wang, S. Dong, N. Sunil, A. Rodriguez, and E. Adelson. Cable manipulation with a tactile-reactive gripper. *The International Journal of Robotics Research*, 40(12-14):1385–1401, 2021.
- [18] Y. Chen, M. Van der Merwe, A. Sipos, and N. Fazeli. Visuo-tactile transformers for manipulation. In *6th Annual Conference on Robot Learning*, 2022.
- [19] C. Sferrazza, Y. Seo, H. Liu, Y. Lee, and P. Abbeel. The power of the senses: Generalizable manipulation from vision and touch through masked multimodal learning. *arXiv preprint arXiv:2311.00924*, 2023.
- [20] J. Pari, N. M. Shafiullah, S. P. Arunachalam, and L. Pinto. The surprising effectiveness of representation learning for visual imitation. *arXiv preprint arXiv:2112.01511*, 2021.
- [21] K. Yu, Y. Han, M. Zhu, and Y. Zhao. Mimictouch: Learning human’s control strategy with multi-modal tactile feedback. *arXiv preprint arXiv:2310.16917*, 2023.
- [22] I. Guzey, B. Evans, S. Chintala, and L. Pinto. Dexterity from touch: Self-supervised pre-training of tactile representations with robotic play. *arXiv preprint arXiv:2303.12076*, 2023.
- [23] F. Sasaki and R. Yamashina. Behavioral cloning from noisy demonstrations. In *International Conference on Learning Representations*, 2020.
- [24] N. M. Shafiullah, Z. Cui, A. A. Altanzaya, and L. Pinto. Behavior transformers: Cloning k modes with one stone. *Advances in neural information processing systems*, 35:22955–22968, 2022.
- [25] A. George and A. B. Farimani. One act play: Single demonstration behavior cloning with action chunking transformers. *arXiv preprint arXiv:2309.10175*, 2023.
- [26] A. Bartsch, A. Car, C. Avra, and A. B. Farimani. Sculptdiff: Learning robotic clay sculpting from humans with goal conditioned diffusion policy. *arXiv preprint arXiv:2403.10401*, 2024.
- [27] T. Z. Zhao, V. Kumar, S. Levine, and C. Finn. Learning fine-grained bimanual manipulation with low-cost hardware. *arXiv preprint arXiv:2304.13705*, 2023.
- [28] C. Chi, S. Feng, Y. Du, Z. Xu, E. Cousineau, B. Burchfiel, and S. Song. Diffusion policy: Visuomotor policy learning via action diffusion. *arXiv preprint arXiv:2303.04137*, 2023.
- [29] J. Ho, A. Jain, and P. Abbeel. Denoising diffusion probabilistic models. *arXiv preprint arxiv:2006.11239*, 2020.
- [30] E. Perez, F. Strub, H. De Vries, V. Dumoulin, and A. Courville. Film: Visual reasoning with a general conditioning layer. In *Proceedings of the AAAI conference on artificial intelligence*, volume 32, 2018.
- [31] N. Rethmeier and I. Augenstein. A primer on contrastive pretraining in language processing: Methods, lessons learned, and perspectives. *ACM Computing Surveys*, 55(10):1–17, 2023.
- [32] A. Radford, J. W. Kim, C. Hallacy, A. Ramesh, G. Goh, S. Agarwal, G. Sastry, A. Askell, P. Mishkin, J. Clark, et al. Learning transferable visual models from natural language supervision. In *International conference on machine learning*, pages 8748–8763. PMLR, 2021.
- [33] J. Kerr, H. Huang, A. Wilcox, R. Hoque, J. Ichnowski, R. Calandra, and K. Goldberg. Self-supervised visuo-tactile pretraining to locate and follow garment features. *arXiv preprint arXiv:2209.13042*, 2022.
- [34] V. Dave, F. Lygerakis, and E. Rueckert. Multimodal visual-tactile representation learning through self-supervised contrastive pre-training. *arXiv preprint arXiv:2401.12024*, 2024.

- [35] M. Zambelli, Y. Aytar, F. Visin, Y. Zhou, and R. Hadsell. Learning rich touch representations through cross-modal self-supervision. In *Conference on Robot Learning*, pages 1415–1425. PMLR, 2021.
- [36] A. George, A. Bartsch, and A. B. Farimani. Openvr: Teleoperation for manipulation. *arXiv preprint arXiv:2305.09765*, 2023.
- [37] K. He, X. Zhang, S. Ren, and J. Sun. Deep residual learning for image recognition. In *Proceedings of the IEEE conference on computer vision and pattern recognition*, pages 770–778, 2016.
- [38] L. Van der Maaten and G. Hinton. Visualizing data using t-sne. *Journal of machine learning research*, 9(11), 2008.
- [39] M. Parakh, A. Fong, A. Simeonov, T. Chen, A. Gupta, and P. Agrawal. Lifelong robot learning with human assisted language planners. In *CoRL 2023 Workshop on Learning Effective Abstractions for Planning (LEAP)*, 2023.